Materials Science & Engineering A 777 (2020) 139052

Contents lists available at ScienceDirect

Materials Science & Engineering A

journal homepage: http://www.elsevier.com/locate/msea

Effects of volume fraction of fine grains on the tensile creep properties of a hot-deformed Mg-Gd-Y-Zr alloy

Yi Yang [a,b], Qinghuan Huo [a,*], Yuxiu Zhang [a], Lu Luo [a], Zhenyu Xiao [a], Jun Wang [b], Aki Hashimoto [c], Xuyue Yang [a,d,**]

[a] Educational Key Laboratory of Nonferrous Metal Materials Science and Engineering, School of Materials Science and Engineering, Central South University, Changsha, 410083, China
[b] Institute for Frontier Materials, Deakin University, Geelong, VIC, 3216, Australia
[c] Technology Div. Nippon Paint Surf Chemicals Co. LTD., 4-1-15 Minamishinagawa, Shinagawa-ku, Tokyo, 140-8675, Japan
[d] Nonferrous Metal Oriented Advanced Structural Materials and Manufacturing Cooperative Innovation Center, Changsha, 410083, China

ARTICLE INFO

Keywords:
Magnesium
Microstructure
Creep
Dislocation

ABSTRACT

The creep properties of a hot-compressed Mg-9Gd-4Y-0.5Zr alloy with different volume fractions (VFs) of fine grains were investigated at 523 K, 548 K and 573 K. Based on the initial VFs of fine grains, the samples were divided into four groups including VF_0 (VF = 0), $VF_{0.2}$ (VF = 20%), $VF_{0.5}$ (VF = 50%) and $VF_{0.8}$ (VF = 80%) samples. The $VF_{0.8}$ sample had the highest yield stress at room temperature, followed by the $VF_{0.5}$ and $VF_{0.2}$ samples, and the VF_0 sample had the lowest. But after creep tests, the $VF_{0.2}$ and $VF_{0.5}$ samples had better creep resistance compared to the VF_0 and $VF_{0.8}$ samples at all the three temperatures. The creep life was shortest for the VF_0 sample due to its lowest yield stress. The $VF_{0.2}$ and $VF_{0.5}$ samples were dominated by dislocation climb and pyramidal <c+a> slip during creep testing. Deformation bands formed by pyramidal <c+a> dislocations and obvious dynamic precipitation strengthened the creep resistance. Besides, the serrated grain boundaries were formed by the combination of coarse and fine grains, which absorbed dislocations and further improved the creep resistance. The $VF_{0.8}$ sample was weakened by the precipitate-free zones (PFZs) formed along the high densities of grain boundaries. Although fine grains could improve yield stress, the excessive fine grains deteriorated the creep resistance owing to the heavy appearance of PFZs. Fortunately, the creep properties were successfully enhanced in this work through introducing mixed microstructures with both coarse and fine grains.

1. Introduction

Magnesium (Mg) and its alloys have been widely used in transportation, aerospace and digital products because of their excellent physical and mechanical characteristics such as low density, high specific stiffness, and damping capacity [1–3]. However, the widespread applications of Mg alloys are restricted due to the low creep resistance at medium to elevated temperatures [4,5]. So far, many attempts have been made to overcome this shortcoming. Adding rare-earth (RE) elements is one of the effective ways [6,7]. RE elements like Gd and Y can increase the heat resistance and promote the precipitation hardening during creep process, leading to a better creep resistance in Mg-Gd-Y based alloys compared to that in RE-free Mg alloys [8,9]. Since RE elements can inevitably delay the occurrence of dynamic recrystallization (DRX) and induce inhomogeneous distributions of grain size during solid solution, hot deformation is usually performed to achieve high volume fractions (VFs) of DRXed grains and high yield stress [10–12]. Similarly, in order to make Mg-Gd-Y based alloy become a good candidate in various industrial fields at medium to elevated temperatures, further improvement for their creep resistance is still in urgent need.

For Mg alloys, the creep mechanisms include self-diffusion, grain boundary slide, dislocation climb, and cross-slip etc., which are dependent on the alloy compositions and service conditions [5,8]. The improvement of creep resistance can be achieved through prohibiting or promoting these mechanisms [13–15]. Generally, alloying and heat

** Corresponding author. Educational Key Laboratory of Nonferrous Metal Materials Science and Engineering, School of Materials Science and Engineering, Central South University, Changsha, 410083, China.
* Corresponding author.
E-mail addresses: huoqinghuan@csu.edu.cn (Q. Huo), yangxuyue@csu.edu.cn (X. Yang).

https://doi.org/10.1016/j.msea.2020.139052
Received 6 June 2019; Received in revised form 3 January 2020; Accepted 3 February 2020
Available online 6 February 2020

treatment are the two common ways. For example, Wan et al. [16] indicated that the creep resistance of Mg-12Zn-4Al alloy could be largely improved by adding only a low content of Ca. The reason was that Ca could catalyze the formation of network phases inside the grain boundaries and the network phases could postpone the crack initiation inside the grain boundaries. Si addition was also found to decrease the creep rate of AZ61 alloy [17]. Although Si could not influence the dominant creep mechanism, the generation of Mg_2Si particles increased the creep resistance through their polygonal morphology and thermostability. Yuan et al. [18] enhanced the creep resistance of Mg-6Gd-4Y-Nd-0.7Zr alloy via artificial aging. The dislocation movement was significantly impeded by the precipitated phases. Besides, in a creative study of pre-creep at 700 K under 5–10 MPa on a Mg-Al binary alloy, the authors found that pre-creep could compel straight grain boundaries evolving into serrated shape [19]. During the next creep tests at 500 K and 600 K, the samples with serrated grain boundaries had much longer creep life in comparison to the samples with straight grain boundaries. Nonetheless, the pre-creep temperature of 700 K is too high for the heat-treatable alloys like Mg-Gd-Y series [20,21]. Moreover, the applied stress range of 5–10 MPa is too low to induce grain boundary slide for multi-element alloys and the pre-creep time is too long for practical applications [22,23]. It is thus expected that an effective and efficient way could be put forward to enhance the creep resistance and prolong the creep life of Mg-Gd-Y based alloys.

In the authors' previous work [24], the microstructure evolutions of a cast Mg-Gd-Y-Zr alloy were studied using both one-step compression and interrupted compression. As a result, the valid methods of attaining microstructures with different VFs (0–80%) of DRXed grains were achieved. Inspired by the previous work [24] and the reference [19], the authors have tried and achieved a novel thought to enhance the creep resistance of Mg-Gd-Y based alloys via inducing serrated grain boundaries and producing mixed microstructures with both coarse and fine grains. Here, in this paper, the tensile creep properties of a Mg-9Gd-4Y-0.5Zr alloy with different VFs of DRXed grains are studied at 523 K, 548 K and 573 K. A novel thought for enhancing creep properties are successfully put forward and the corresponding reasons are explained by creep kinetics analysis and various microstructural characterizations. It is hoped that the novel thought in this work can contribute to the theories and applications of heat-resistant Mg-RE based alloys.

2. Experimental procedure

The Mg alloy with an element composition of 9 Gd, 4 Y, 0.5 Zr and balanced Mg (all in weight percentage) was prepared through semi-continuous casting. Cubic samples with a gauge size of 10 × 10 × 12 mm^3 were cut from the ingot center. Solid solution was performed at 793 K for 8 h and then air cooling, leading to the evolution of a microstructure composed of equiaxed grains with an average grain size of ~200 μm.

Hot compression was carried out at 793 K using an Instron-type mechanical testing machine. Three terminative true strains were determined, including $\varepsilon = 0.3$, 1.2 and 1.6. The samples were subjected to the same deformation method as the authors' previous study, including a traditional one-step compression and an interrupted compression [24,25]. The true strains to $\varepsilon = 0.3$ and 1.2 were obtained using one-step compression at a strain rate of $\dot{\varepsilon} = 3 \times 10^{-3}\ s^{-1}$. While the true strain of $\varepsilon = 1.6$ were obtained using interrupted compression, including compression to a true strain of $\varepsilon = 0.3$ at a strain rate of $\dot{\varepsilon} = 3 \times 10^{-3}\ s^{-1}$, intermediate annealing at 793 K for 10 min, and followed by compression to the terminative true strain of $\varepsilon = 1.6$ at a high strain rate of $\dot{\varepsilon} = 3 \times 10^{-1}\ s^{-1}$. In this way, the VF of DRXed grains could get to 80%, otherwise RE elements would delay the DRX process during the one-step compression [24–26]. After each hot deformation, water quenching was performed within 1.5 s to preserve the instantaneous deformed microstructure. For each testing condition, three specimens were used to calculate the average values of the VFs of fine grains. The average grain size of the obtained fine grains during deformation was around 10 μm. Hereafter, the samples are divided into four groups according to their VFs of fine grains, which are VF = 0 ($\varepsilon = 0$), VF = 0.2 ($\varepsilon = 0.3$), VF = 0.5 ($\varepsilon = 1.2$) and VF = 0.8 ($\varepsilon = 1.6$). For briefness, the four groups of samples are labeled as VF_0, $VF_{0.2}$, $VF_{0.5}$, and $VF_{0.8}$ samples, respectively.

Uniaxial tensile tests were carried out at room temperature with a strain rate of $3 \times 10^{-3}\ s^{-1}$. Tensile creep tests were conducted through an RWS-50 electronic creep testing machine at 523 K, 548 K and 573 K under different applied stresses. The tensile direction was perpendicular to the hot compressive direction. Samples for uniaxial tensile tests and tensile creep tests were machined with a gauge size of 5 × 1.5 × 1 mm^3. Before creep tests, the samples were pre-heated to the corresponding creep temperature and held for 10 min. After creep tests, the samples were immediately quenched in water. The microstructures before and after creep tests were examined using optical microscopy (OM), scanning electron microscopy (SEM), electron backscatter diffraction (EBSD) apparatus with orientation imaging microscopy (OIM), and transmission electron microscopy (TEM). Samples for OM, SEM and EBSD observations were cut from the center of the tested specimens, followed by mechanically grinded on sand papers from 400 # to 1600 # and electropolishing in a solution of nitric acid (10 mL) and absolute ethanol (100 mL). The preparation of TEM samples involved ion milling method after mechanical grinding to a thickness of 100 μm. All the observation directions were along the hot compressive direction.

3. Results

3.1. Initial microstructures and uniaxial tensile properties

Fig. 1 presents the initial microstructures of the VF_0, $VF_{0.2}$, $VF_{0.5}$, and $VF_{0.8}$ samples. The initial grains of the VF_0 sample (Fig. 1(a)) are gradually fragmented and straight grain boundaries are apparently serrated as the compressive strain increases to $\varepsilon = 0.3$ and $\varepsilon = 1.2$ (Figs. 1(b) and (c)). Fine grains are successively formed as colonies along the initial grain boundaries, resulting in the $VF_{0.2}$ and $VF_{0.5}$ samples owning microstructures with mixed grain sizes and serrated grain boundaries. When the true strain is increased to $\varepsilon = 1.6$, DRX happens in most regions and the serrated grain boundaries tend back to straight shape in the $VF_{0.8}$ sample. No obvious dynamic precipitation happens in the VF_0, $VF_{0.2}$ and $VF_{0.5}$ samples while a low extent of dynamic precipitation happens in the $VF_{0.8}$ sample. Therefore, dynamic precipitation during hot compression acts a minor role in the following uniaxial tensile tests and tensile creep tests.

The typical inverse pole figure (IPF) maps of initial microstructures are presented in Fig. 2. Different colors indicate different crystallographic orientations, for example, red grains represent their *c*-axes parallel to the compressive direction. Black lines represent high angle boundaries (HABs) with misorientations over 15° and white lines represent low angle boundaries (LABs) with misorientations ranging from 2° to 15°. It is seen that the initial grains in the VF_0 sample (Fig. 2 (a)) show random orientations. After hot compression, DRX happens and fine grains are created with random orientations in the $VF_{0.2}$, $VF_{0.5}$ and $VF_{0.8}$ samples. Most of their residual initial grains are rotated to have their *c*-axes parallel to the compressive direction (Fig. 2(b)–(d)). Within the red colored grains, LABs are formed and some of the LABs are penetrating across the whole grains.

Fig. 3 shows the typical kernel average misorientation (KAM) maps of initial microstructures. As can be seen, the VF_0 sample has an undistorted microstructure. With the compressive strain increasing, the residual stress firstly increases and then decreases. Moreover, the residual stress mostly exists in residual initial grains and matches the positions of LABs in Fig. 2 very well. These stable LABs during hot compression are considered as deformation bands or kink bands, which are usually treated as the primary factor for continuous DRX in hot-

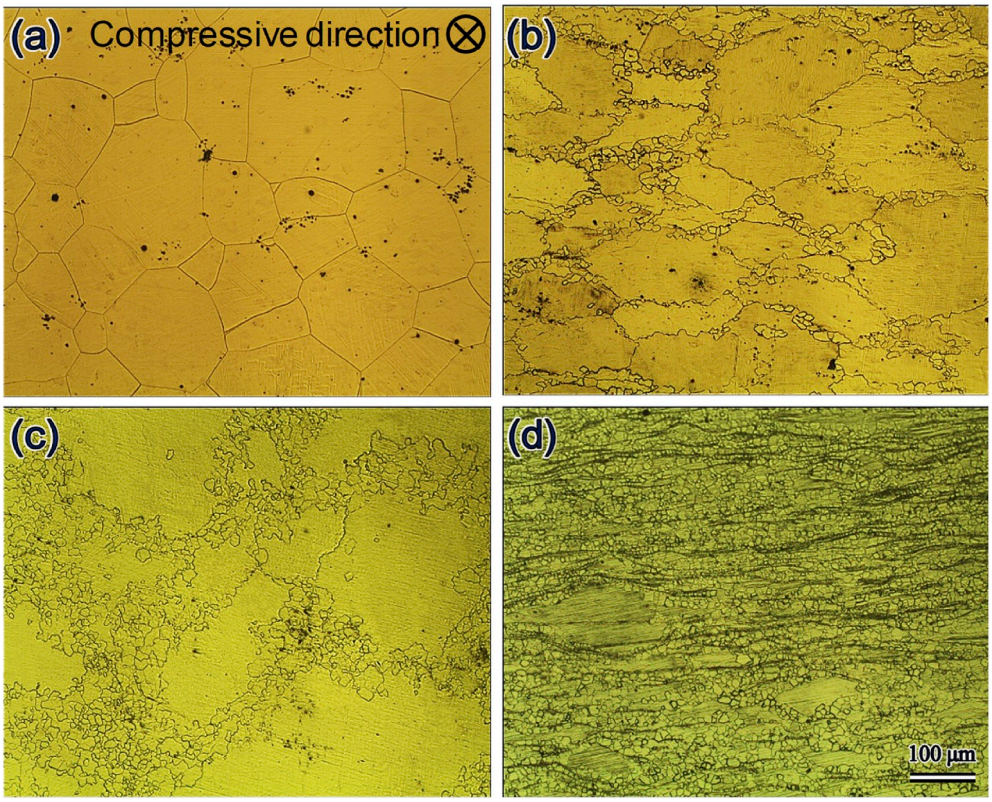

Fig. 1. Initial microstructures of (a) VF_0, (b) $VF_{0.2}$, (c) $VF_{0.5}$ and (d) $VF_{0.8}$ samples. Observation direction is along hot compression direction.

deformed Mg alloys [24–29].Fig. 4 shows the resultant mechanical properties after uniaxial tensile tests in triplicate. As can be seen, the $VF_{0.8}$ sample has the highest yield stress due to the high VF of DRXed grains [28]. The yield stresses of the samples, all measured as the 0.2% proof stresses, are 116 MPa for the VF_0 sample, 143 MPa for the $VF_{0.2}$ sample, 174 MPa for the $VF_{0.5}$ sample and 232 MPa for the $VF_{0.8}$ sample, respectively. The applied stresses for tensile creep tests are then determined lower than the yield stress of the VF_0 sample. The other mechanical properties at room temperature are listed in Table 1.

3.2. Creep properties

Fig. 5 shows the typical creep curves for the four groups of samples tested at 523 K, 548 K and 573 K under the applied stress of 100 MPa. It can be obviously observed from the creep curves that the VF_0 sample has a short creep life and the $VF_{0.8}$ sample has a high creep rate at all the three creep temperatures. The specific steady creep rates of the samples tested under 100 MPa are listed in Tables 2–4, respectively. For brevity, the steady creep rates under other applied stresses are also listed in the tables instead of further enumeration. It is noteworthy that the $VF_{0.5}$ sample shows the best creep resistance and followed by the $VF_{0.2}$ sample at 523 K and 548 K while the $VF_{0.2}$ sample owns the best creep resistance at 573 K. This switched phenomenon of the creep resistance between the $VF_{0.2}$ and $VF_{0.5}$ samples is interesting, which will be discussed later. With the results shown in Fig. 5 and listed in Tables 2–4, it can be suggested that the samples with mixed grain sizes have better creep resistance compared to the fine-grained sample and the coarse-grained sample. Namely, the best microstructure conducive to creep properties does not exists in the sample which has the highest yield stress. This is a new finding in heat-resistant Mg alloys and it is also worthy of explaining the detailed reasons later.

It is essential to speculate the possible creep mechanisms for understanding the different creep properties in the tested samples. The stress exponent, n, which represents the sensibility of creep rate to stress variation at a certain temperature and corresponds to the specific creep mechanism, can be obtained by taking the creep time derivative from the creep curves [30]. Specifically, for Mg alloys, an n value ~1 stands for the creep process controlled by self-diffusion, ~2 for grain boundary slide, ~3 for dislocation viscous glide, ranging from 4 to 7 for dislocation climb or cross-slip [16,30]. The steady creep rate can be expressed by the conventional power-law equation in accordance with the applied stress σ and the absolute temperature T [31,32]:

$$\dot{\varepsilon} = A\sigma^{n}\exp\left(-\frac{Q}{RT}\right) \tag{1}$$

where A is a constant, Q is the activation energy for creep and R is the gas constant. When the T is constant, the equation can be modified as:

$$n = \frac{\partial \ln \dot{\varepsilon}}{\partial \ln \sigma} \tag{2}$$

The stress exponent, n, can be obtained from the slope of a ln-ln plot of steady creep rate versus applied stress. Based on the results in Fig. 5 and Tables 2–4, three plots of creep stress exponents are shown in Fig. 6. At 523 K and 548 K, as shown in Figs. 6(a) and (b), the stress exponents of the VF_0, $VF_{0.2}$ and $VF_{0.5}$ samples are all around or above 4, indicating that their creep mechanisms may be dislocation climb or cross-slip [32]. Nonetheless, the stress exponent of the $VF_{0.8}$ sample appears to be around 2, suggesting the main creep mechanism of the $VF_{0.8}$ sample is grain boundary slide [30]. Similarly, the creep stress exponents at 573 K exhibited in Fig. 6(b) still have the lowest n value in the $VF_{0.8}$ sample. Since the n values are approximate at all the three temperatures, the corresponding creep mechanisms should be the same. Meanwhile, the activation energy, Q, for all samples crept under 100 MPa is calculated and shown in Fig. 7. Compared to the self-diffusion energy in Mg (135 kJ/mol), the main creep mechanism is dislocation slip for the VF_0, $VF_{0.2}$ and $VF_{0.5}$ samples and grain boundary slide for the $VF_{0.8}$ sample [30–32]. Accordingly, the OM, SEM and TEM observations are all performed on the samples crept at 523 K. Moreover, the longer creep life at

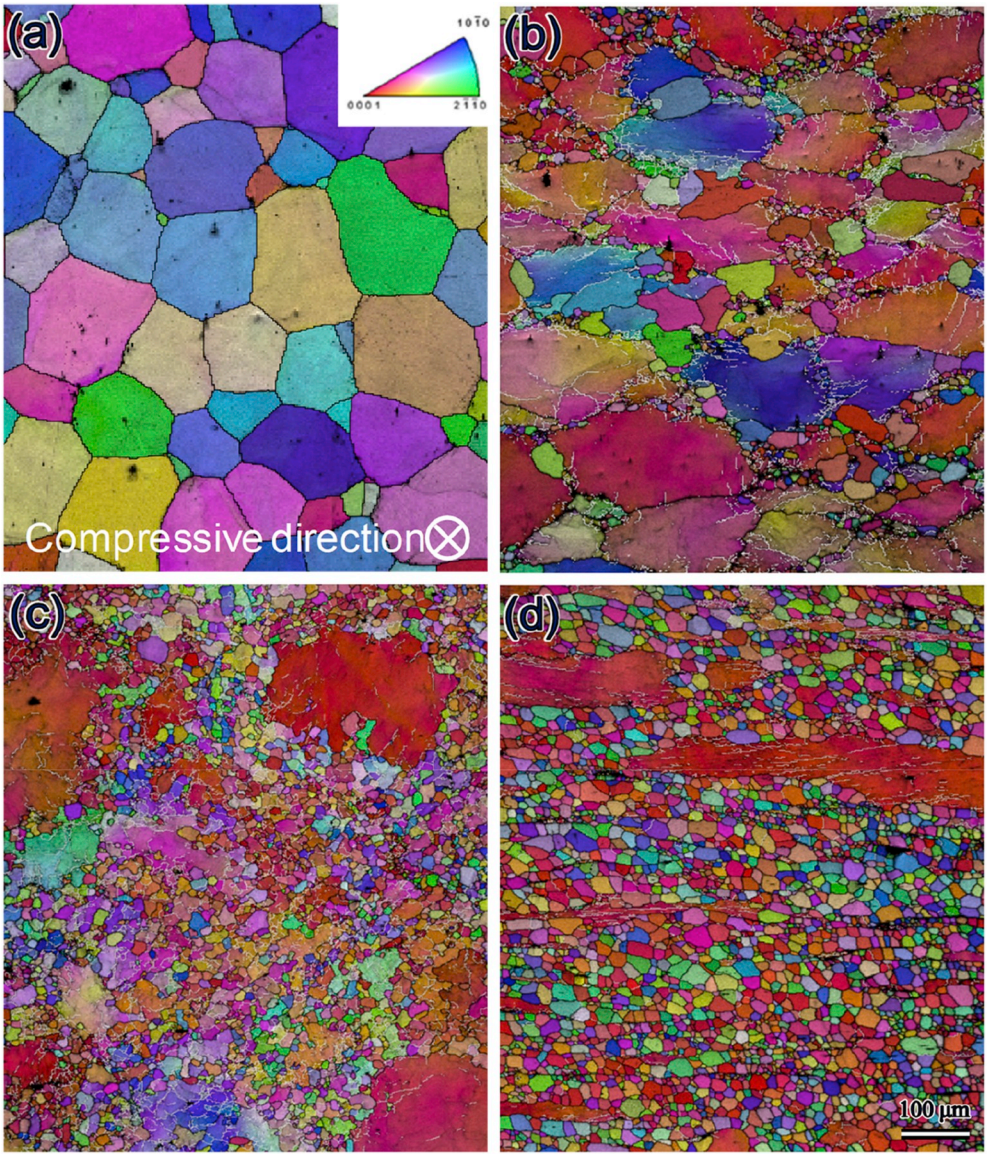

Fig. 2. Typical IPF maps of initial microstructures of (a) VF_0, (b) $VF_{0.2}$, (c) $VF_{0.5}$ and (d) $VF_{0.8}$ samples. Black lines represent grain boundaries with high angle misorientations above 15° while white lines represent low angle boundaries with misorientations between 2° and 15°. Observation direction is along hot compression direction.

523 K can improve the accuracy of microstructural characterization.

4. Discussion

4.1. Microstructure evolutions during creep testing

Judging from the above, it is obvious that the $VF_{0.2}$ and $VF_{0.5}$ samples own better creep properties at all the three temperatures. It is necessary to find the crack areas in the four groups of samples. Fig. 8 shows the microstructures of the samples crept at 523 K under 100 MPa. When the VF_0 sample crept to 50 h, there are evident cracks (indicated by the red arrows) propagating in the grain interiors in Fig. 8(a). Although the grain boundaries are still straight, the VF_0 sample fails due to its low yield stress in a short time, which is not even long enough for strain aging to happen [31,33]. In the $VF_{0.2}$ sample, a few cracks can be found in the sites of DRXed nucleation (Figs. 8(b) and (c)). These sites are surrounded by initial coarse grains, indicating that fine grains prefer to acting as crack site during creep process [33,34]. This is in agreement with many other researches about the creep properties in steel and Ni alloys [35–38]. In the $VF_{0.5}$ sample, as shown in Figs. 8(d) and (e), the cracks are also found in the areas of fine grains. Considering the similar *n* values (corresponding to the main creep mechanism of dislocation slip) but different creep properties in the VF_0, $VF_{0.2}$ and $VF_{0.5}$ samples, an interesting suggestion can be proposed here. The serrated grain boundaries formed by coarse and fine grains can continuously absorb dislocations during creep process, since serrated grain boundaries tend to evolve back into straight shape [19,38]. These grain boundaries remain the serrated shape stably even the creep approximately reaches rupture as presented by Fig. 8(b)–(e). In contrast, in Fig. 8(f), the high VF of fine grains leads to very few serrated grain boundaries in the $VF_{0.8}$ sample. Grain boundary slide happens rapidly and crack sites are easily increased [39].

4.2. Precipitation behaviors during creep testing

To further study the influences of different microstructures on the creep properties, it is also necessary to analyze the precipitation behaviors during creep testing. Since OM maps cannot clearly show

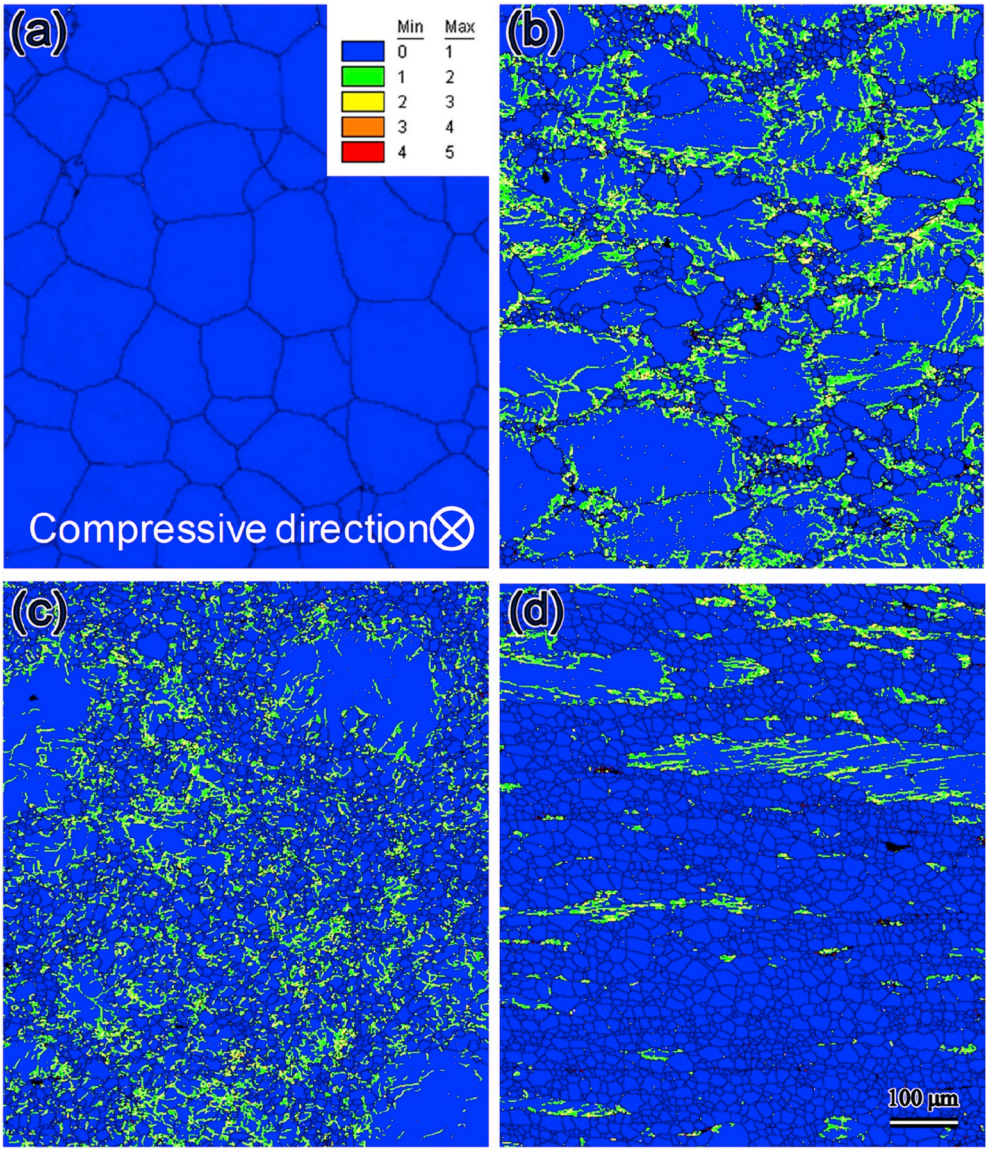

Fig. 3. Typical KAM maps of initial microstructures of (a) VF_0, (b) $VF_{0.2}$, (c) $VF_{0.5}$ and (d) $VF_{0.8}$ samples. Observation direction is along hot compression direction.

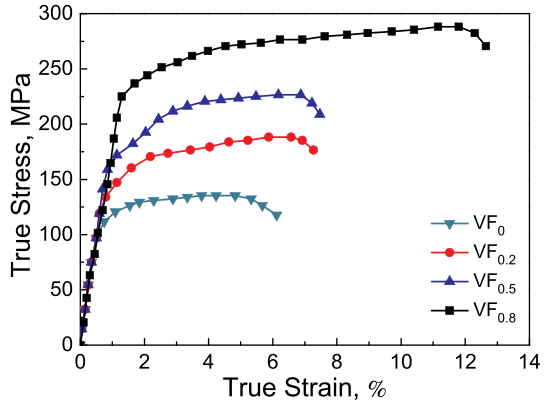

Fig. 4. True stress-strain curves of samples tensile tested at room temperature.

dynamic precipitates, the occurrence of dynamic precipitation needs to be proven by SEM observation. The typical SEM images of the $VF_{0.2}$, $VF_{0.5}$ and $VF_{0.8}$ samples crept at 523 K under 100 MPa after 100 h are shown in Fig. 9. It can be seen in Fig. 9(a) that many needle-like

Table 1
Results of uniaxial tensile tests at room temperature.

Properties	VF_0	$VF_{0.2}$	$VF_{0.5}$	$VF_{0.8}$
Yield stress /MPa	116	143	174	232
Ultimate tensile stress /MPa	135	188	226	288
Fracture elongation /%	6.1	7.3	7.5	12.6

precipitates are formed in the $VF_{0.2}$ sample and the precipitates are crossing each other by an angle of 60°. Besides dynamic precipitation in the $VF_{0.2}$ sample, Fig. 9(b) shows the formation of deformation bands which are the LABs in the residual coarse grains in Fig. 2(b). The deformation bands can promote cDRX during hot compression, improve yield stress at room temperature, trigger dynamic precipitation and strengthen creep resistance [40,41]. However, in the $VF_{0.5}$ sample (Fig. 9(c)), PFZs are generated along the fine grain boundaries. In Fig. 9 (d), the PFZs becomes wider and owns a higher density owing to grain boundary slide being the main creep mechanism of the $VF_{0.8}$ sample. As PFZs are usually treated as the weak-strength areas perpendicular or having large tilt angles to the tensile creep direction [34,42,43], the creep resistance of the $VF_{0.8}$ sample is much lower compared to the $VF_{0.2}$

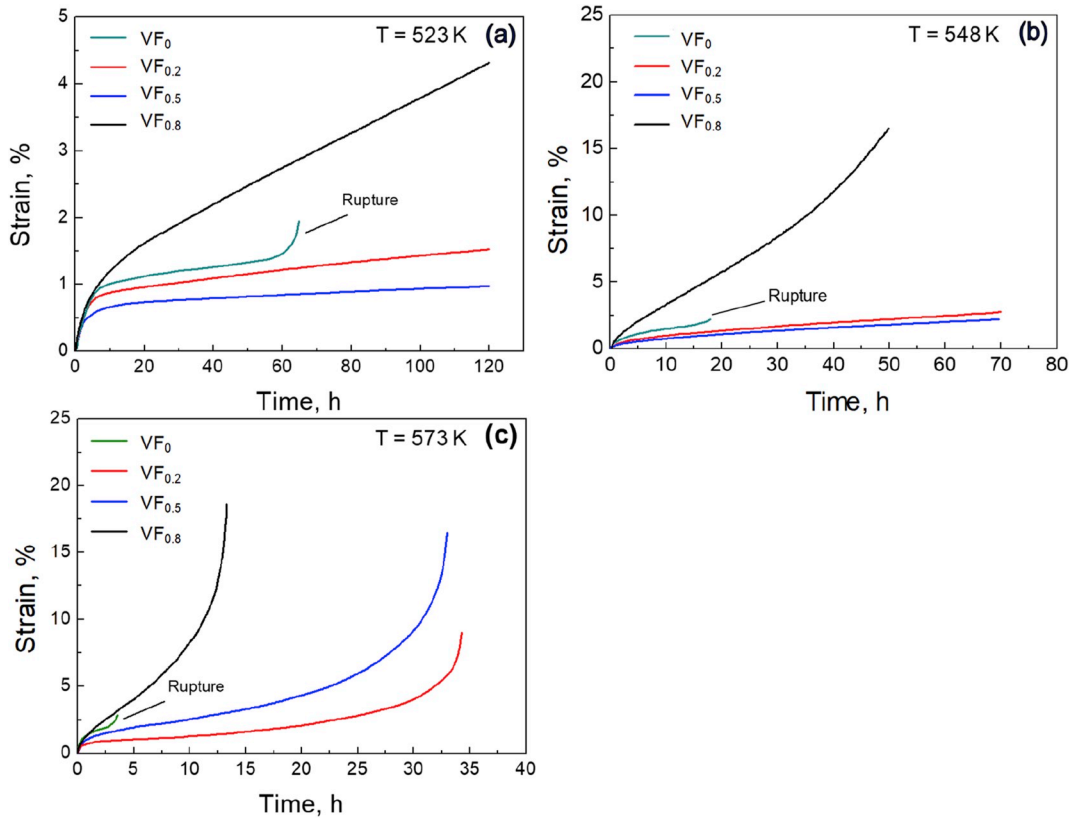

Fig. 5. Creep curves of samples crept at (a) 523 K, (b) 548 K and (c) 573 K under 100 MPa.

Table 2
Steady creep rate of samples crept at 523 K.

Applied stress	VF_0	$VF_{0.2}$	$VF_{0.5}$	$VF_{0.8}$
60 MPa	1.97×10^{-8} s^{-1}	1.90×10^{-8} s^{-1}	8.24×10^{-9} s^{-1}	1.38×10^{-7} s^{-1}
70 MPa	3.57×10^{-8} s^{-1}	2.41×10^{-8} s^{-1}	9.27×10^{-9} s^{-1}	1.67×10^{-7} s^{-1}
80 MPa	5.29×10^{-8} s^{-1}	3.66×10^{-8} s^{-1}	1.28×10^{-8} s^{-1}	2.52×10^{-7} s^{-1}
90 MPa	7.21×10^{-8} s^{-1}	5.81×10^{-8} s^{-1}	2.06×10^{-8} s^{-1}	3.12×10^{-7} s^{-1}
100 MPa	1.09×10^{-7} s^{-1}	9.03×10^{-8} s^{-1}	3.41×10^{-8} s^{-1}	3.75×10^{-7} s^{-1}

Table 3
Steady creep rate of samples crept at 548 K.

Applied stress	VF_0	$VF_{0.2}$	$VF_{0.5}$	$VF_{0.8}$
60 MPa	7.04×10^{-8} s^{-1}	4.03×10^{-8} s^{-1}	2.94×10^{-8} s^{-1}	6.47×10^{-7} s^{-1}
70 MPa	1.42×10^{-7} s^{-1}	7.80×10^{-8} s^{-1}	5.67×10^{-8} s^{-1}	8.67×10^{-7} s^{-1}
80 MPa	2.50×10^{-7} s^{-1}	1.09×10^{-7} s^{-1}	8.80×10^{-8} s^{-1}	1.12×10^{-6} s^{-1}
90 MPa	4.90×10^{-7} s^{-1}	1.78×10^{-7} s^{-1}	1.49×10^{-7} s^{-1}	1.43×10^{-6} s^{-1}
100 MPa	7.61×10^{-7} s^{-1}	3.40×10^{-7} s^{-1}	2.41×10^{-7} s^{-1}	1.88×10^{-6} s^{-1}

and $VF_{0.5}$ samples. Some fine grain interiors have very few and tiny precipitates. Previous reports put forward that the strength is lower along grain boundary than in grain interior at high temperature [32, 44–50]. Vacancies are always formed along grain boundaries due to the

Table 4
Steady creep rate of samples crept at 573 K.

Applied stress	VF_0	$VF_{0.2}$	$VF_{0.5}$	$VF_{0.8}$
60 MPa	2.30×10^{-7} s^{-1}	9.62×10^{-8} s^{-1}	1.96×10^{-7} s^{-1}	2.72×10^{-6} s^{-1}
70 MPa	4.72×10^{-7} s^{-1}	2.41×10^{-7} s^{-1}	2.81×10^{-7} s^{-1}	4.10×10^{-6} s^{-1}
80 MPa	1.12×10^{-6} s^{-1}	2.70×10^{-7} s^{-1}	5.02×10^{-7} s^{-1}	4.65×10^{-6} s^{-1}
90 MPa	2.63×10^{-6} s^{-1}	4.85×10^{-7} s^{-1}	1.29×10^{-6} s^{-1}	5.59×10^{-6} s^{-1}
100 MPa	4.57×10^{-6} s^{-1}	1.16×10^{-6} s^{-1}	1.69×10^{-6} s^{-1}	8.04×10^{-6} s^{-1}

easy grain boundary slide. Then, the dynamic precipitates are likely to dissolve into the Mg matrix, which is the precipitate re-dissolution [32, 44,51]. With the continuous occurrence of precipitate re-dissolution, PFZs are gradually formed and tend to widen along grain boundaries of fine grains. The low-density and tiny-scale precipitates and the wide PFZs observed in fine grains can further prove the serious grain boundary slide and the resultant poor creep resistance of the $VF_{0.8}$ sample.

Hence, serrated grain boundaries absorbing dislocations and deformation bands strengthening the residual coarse grains can effectively enhance creep properties, but the formation of PFZs in the fine grains severely deteriorates creep properties. Mixed microstructures containing suitable VFs of coarse grains and fine grains enhancing the creep properties is the most important finding in this work.

4.3. *Dislocation slip during creep testing*

To better understand the primary causes for the differences between creep properties of the $VF_{0.2}$ and $VF_{0.5}$ samples, TEM observations are

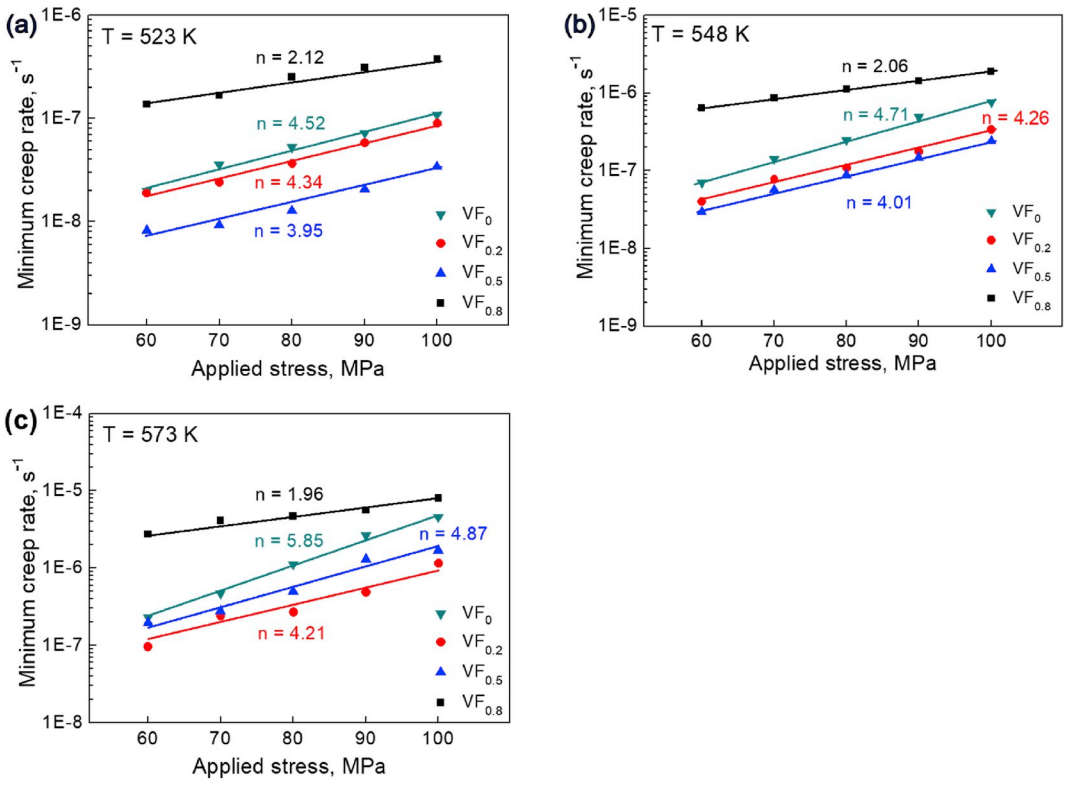

Fig. 6. Ln-ln plots of steady creep rate versus applied stress of samples crept at (a) 523 K, (b) 548 K and (c) 573 K.

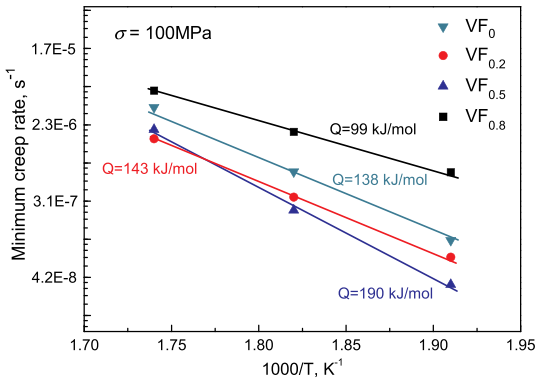

Fig. 7. Plots of minimum creep rate versus 1000/T for all samples.

performed. Fig. 10 presents the bright fields of typical areas in the $VF_{0.2}$ and $VF_{0.5}$ samples crept at 523 K under 100 MPa for 100 h. Two-beam mode is taken for the observation of the $VF_{0.2}$ sample in Figs. 10(a) and (b). The incident beam direction is $\boldsymbol{B} = [01\bar{1}0]$. Under this condition, all the basal planes are edge on. When the diffraction vector is $\boldsymbol{g} = [2\bar{1}\bar{1}0]$, as shown in Fig. 10(a), <c> dislocations are all extinct based on the $\boldsymbol{g}\cdot\boldsymbol{b}$ criterion [52]. There are some short trails of dislocations lying on the basal planes and perpendicular to the dynamic precipitates. Since whole basal dislocations should have a long and thin shape and a dispersed distribution, the short trails are confirmed as edge <a> dislocations climbing from one basal plane to the adjacent basal plane [35]. Meanwhile, an elongated structure (surrounded by the two blue dash lines) is penetrated by precipitates. It is the deformation band existing in the residual coarse grain. To avoid the contrast effect brought by precipitates and to manifest the dislocation component of deformation band, Fig. 10(b) shows the bright field under the diffraction vector $\boldsymbol{g} = [0002]$. Under this condition, all <a> dislocations are extinct and the contrast of precipitates becomes light [39,53]. It is clearly seen that the deformation band contains masses of <c> dislocations. Due to <c> dislocations are sessile, <a> dislocations must exist in the deformation band [54,55]. Namely, the deformation band are the arrays of pyramidal <c+a> dislocations. The hard observation of <a> dislocations are possibly because of the much larger scale of precipitates in comparison to the short length of <a> dislocations. Fig. 10(c) shows the bright field of the $VF_{0.5}$ sample crept at 523 K under 100 MPa for 100 h. Under the incident beam direction $\boldsymbol{B} = [2\bar{1}\bar{1}0]$, dislocations are observed to gather as clusters and distribute parallel to the basal plane trace, which are also the typical characterization of dislocation climb [35,56]. Thus, it can be concluded from the stress exponents and the TEM observations that the main creep mechanisms of the $VF_{0.2}$ and $VF_{0.5}$ samples are dislocation climb and pyramidal <c+a> slip.

Another equally important thing is the switched creep resistance between the $VF_{0.2}$ and $VF_{0.5}$ samples at the three creep temperatures, as depicted in Fig. 5. Taking into account that the main creep mechanisms of the $VF_{0.2}$ and $VF_{0.5}$ samples are alike, the reason is probably lying on the different VFs of fine grains and the following formation of PFZs. Two TEM bright fields of the $VF_{0.2}$ and $VF_{0.5}$ samples crept at 523 K under 100 MPa after 100 h are taken and shown in Fig. 11. Obvious PFZs can be found in both the $VF_{0.2}$ and $VF_{0.5}$ samples. The incident beam direction is $\boldsymbol{B} = [01\bar{1}0]$ for the $VF_{0.2}$ sample in Fig. 11(a) and the PFZ width is roughly 280 nm, while the incident beam direction is $\boldsymbol{B} = [2\bar{4}2\bar{3}]$ for the $VF_{0.5}$ sample in Fig. 11(b) and the PFZ width is around 520 nm (nearly 2 times of the PFZ width in the $VF_{0.2}$ sample). Since the formation of PFZs is caused by grain boundary slide of fine grains, the higher VF of fine grains in the $VF_{0.5}$ sample leads to the wider PFZs in Fig. 11(b). As the length of one <a> dislocation is 0.32 nm [11], the wider PFZs in the $VF_{0.5}$ sample store higher densities of dislocations and induce more serious stress concentration. Although the higher yield stress of the $VF_{0.5}$ sample can compensate the creep resistance, a lower creep resistance is still obtained at 573 K due to the atomic diffusion rate would be more easily triggered and the PFZs would be wider in the $VF_{0.5}$ sample [8]. Additionally, the lowest yield stress can hardly compensate

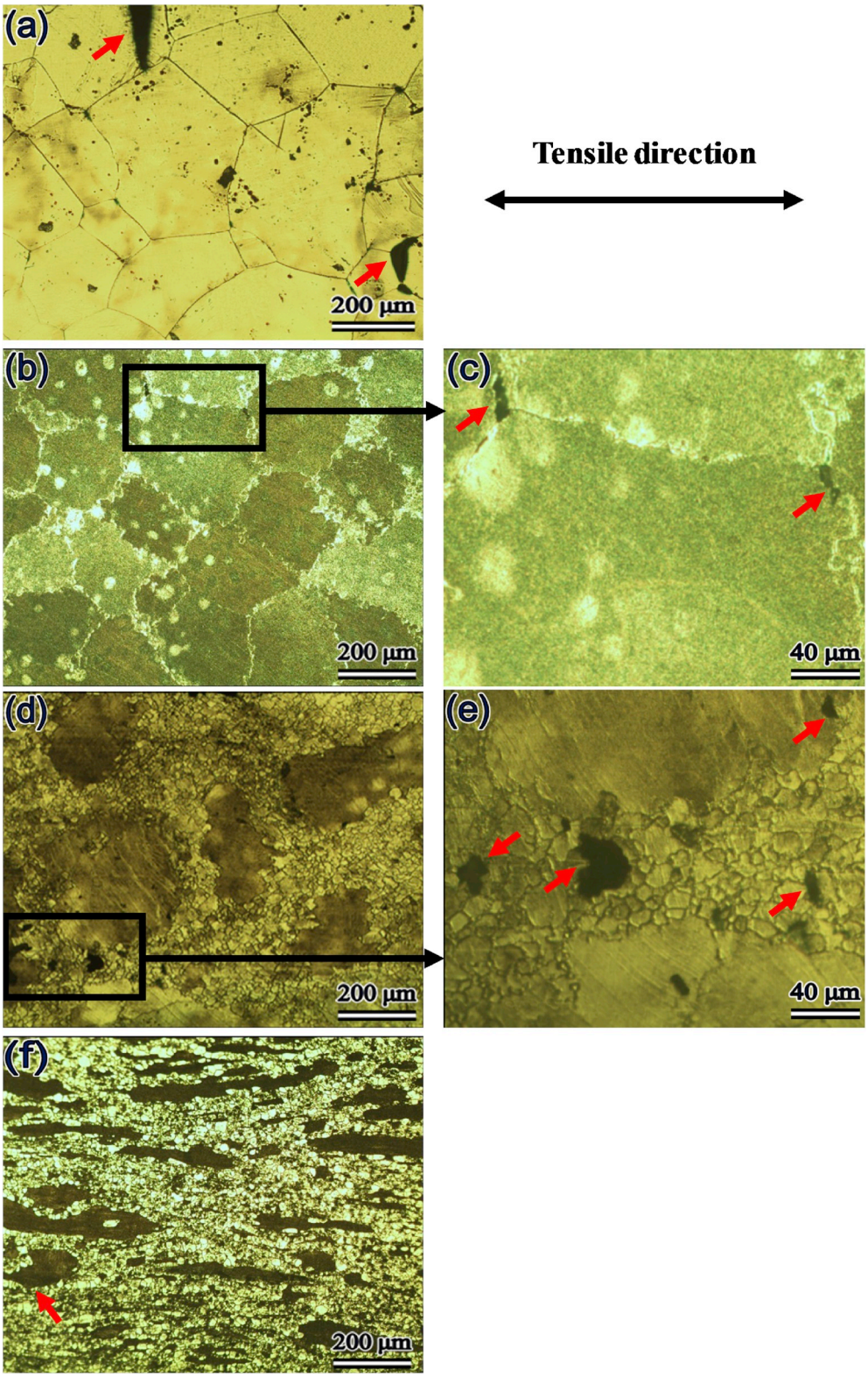

Fig. 8. Microstructures of samples crept at 523 K under 100 MPa: (a) VF_0 sample crept for 50 h, (b), (c) $VF_{0.2}$, (d), (e) $VF_{0.5}$ and (f) $VF_{0.8}$ samples crept for 100 h (Red arrows indicate cracks.). (For interpretation of the references to color in this figure legend, the reader is referred to the Web version of this article).

the short creep life of the VF_0 sample although PFZ is rarely formed in coarse grains at all the three temperatures. And the creep resistance of the $VF_{0.8}$ sample is further deteriorated at 573 K owing to more serious grain boundary slide.

5. Conclusions

The tensile creep properties of a hot-compressed Mg-9Gd-4Y-0.5Zr alloy with different initial microstructures are investigated at 523 K, 548 K and 573 K under a wide range of applied stress. Based on the VFs

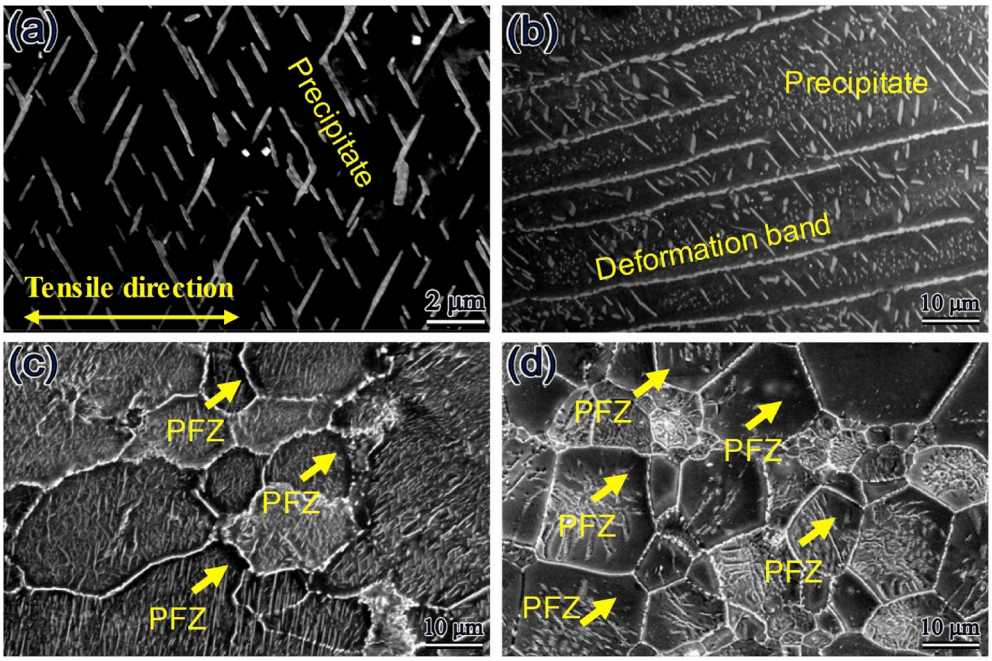

Fig. 9. Typical SEM images of (a), (b) $VF_{0.2}$, (c) $VF_{0.5}$, and (d) $VF_{0.8}$ samples after crept at 523 K under 100 MPa for 100 h.

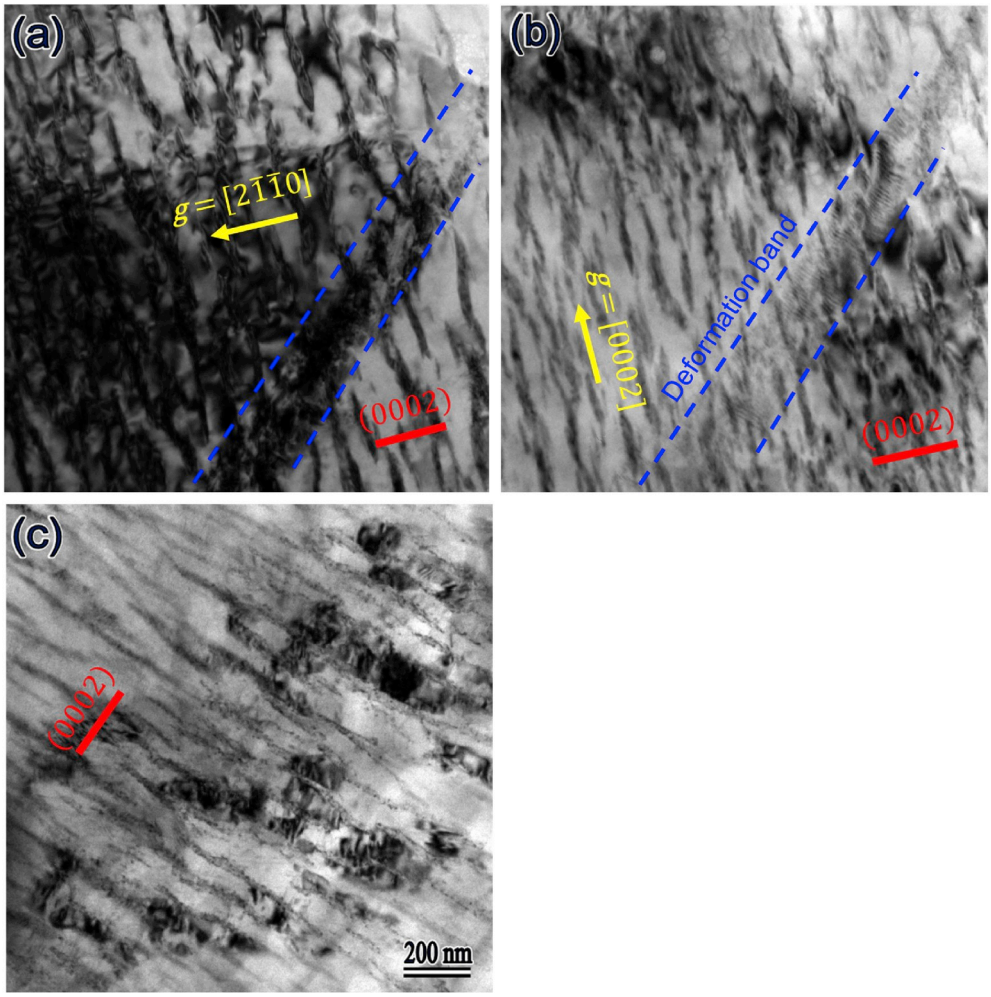

Fig. 10. TEM bright fields of (a), (b) $VF_{0.2}$ and (c) $VF_{0.5}$ samples after crept at 523 K under 100 MPa for 100 h. Incident beam directions are (a), (b) $\boldsymbol{B} = [01\bar{1}0]$ and (c) $\boldsymbol{B} = [2\bar{1}\bar{1}0]$.

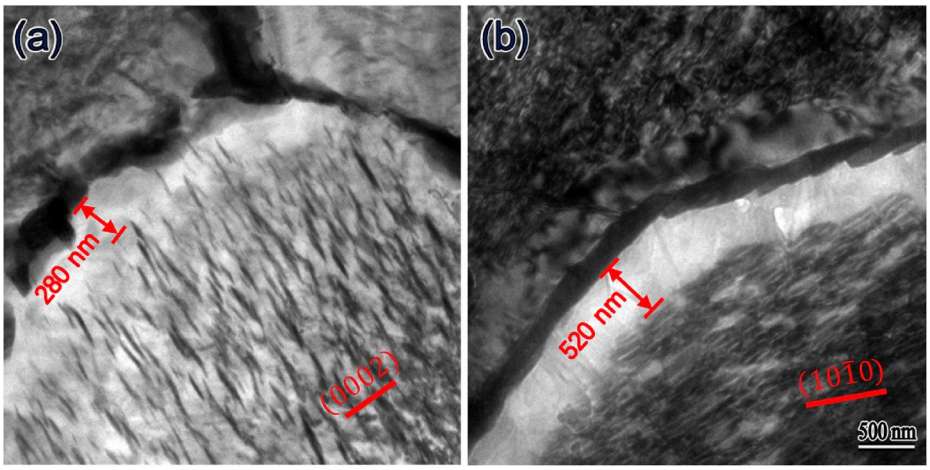

Fig. 11. TEM bright fields of precipitate-free zones in (a) $VF_{0.2}$ and (b) $VF_{0.5}$ samples after crept at 523 K under 100 MPa for 100 h. Incident beam directions are (a) $\boldsymbol{B} = [01\bar{1}0]$ and (b) $\boldsymbol{B} = [2\bar{4}2\bar{3}]$.

of DRXed grains after hot compression, the samples are classified into four groups: VF_0, $VF_{0.2}$, $VF_{0.5}$ and $VF_{0.8}$ samples, which correspond to the VFs of 0, 0.2, 0.5 and 0.8, respectively. The main conclusions obtained from tensile creep tests and microstructural characterizations are summarized as follows:

(1) Due to the low yield stress, the VF_0 sample is lacking a hardening effect during creep testing. The crack initiation is early and the creep life is short for the VF_0 sample. Due to the high VF of fine grains, the $VF_{0.8}$ sample is dominated by grain boundary slide and the PFZs are easily generated during creep testing. The high-density PFZs in the $VF_{0.8}$ sample leads to a low creep resistance regardless of the high yield stress.
(2) The main creep mechanisms of the $VF_{0.2}$ and $VF_{0.5}$ samples are dislocation climb and pyramidal $<c+a>$ slip. The evident dynamic precipitation and deformation bands composed by pyramidal $<c+a>$ dislocations strengthen the creep resistance. Besides, serrated grain boundaries are formed by the combination of coarse and fine grains, which can absorb dislocations to further improve the creep resistance.
(3) At all the three temperatures, the $VF_{0.2}$ and $VF_{0.5}$ samples acquire better creep properties compared to the VF_0 and $VF_{0.8}$ samples. Particularly, the creep resistance of the $VF_{0.5}$ sample is higher at 523 K and 548 K but lower at 573 K compared to that of the $VF_{0.2}$ sample. This switch is caused by the easier formation of PFZs with the increased creep temperature.
(4) Although high VFs of fine grains could improve yield stress, excessive fine grains undermine the creep properties due to easy grain boundary slide and heavy appearance of PFZs. Fortunately, this work successfully presents an efficient and economical method to improve creep properties through introducing mixed microstructures with both coarse and fine grains.

Data availability statement

The raw and processed data required to reproduce these findings cannot be shared at this moment due to technical and time limitations.

Originality statement

The authors confirm that the article has not been submitted to peer review, nor has been accepted for publishing in another journal. The authors also confirm that the research in this work is original, and that all the data given in the article are real and authentic. If necessary, the article can be recalled, and errors corrected.

Declaration of competing interest

The authors declare that they have no known competing financial interests or personal relationships that could have appeared to influence the work reported in this paper.

CRediT authorship contribution statement

Yi Yang: Methodology, Writing - original draft, Writing - review & editing. **Qinghuan Huo:** Formal analysis, Conceptualization, Supervision, Funding acquisition. **Yuxiu Zhang:** Investigation. **Lu Luo:** Investigation. **Zhenyu Xiao:** Investigation. **Jun Wang:** Investigation. **Aki Hashimoto:** Investigation. **Xuyue Yang:** Conceptualization, Supervision, Funding acquisition.

Acknowledgements

The authors gratefully acknowledge the financial supports received from the National Natural Science Foundation of China (Grants No. 51974376, 51771230 and U1864209), the Natural Science Foundation of Hunan Province (Grant No. 2019JJ40376), the Key Research Program of Hunan Province (Grant No. 2019WK2062) and the Distinguished Professor Project of Central South University (Grant No. 202045009).

References

[1] J.J. Kim, D.S. Han, Recent development and applications of magnesium alloys in the hyundai and Kia motors corporation, Mater. Trans. 49 (2008) 894–897.
[2] Q. Huo, X. Yang, J. Wang, H. Sun, J. Guo, L. Jiang, Mechanical behavior and deformation mechanisms of AZ31 Mg alloy at liquid nitrogen temperature, Mater. Lett. 109 (2013) 78–82.
[3] Q. Huo, D. Ando, Y. Sutou, J. Koike, Stress-strain hysteresis and strain hardening during cyclic tensile test of Mg-0.6at%Y alloy, Mater. Sci. Eng. A 678 (2016) 235–242.
[4] M.R. Barnett, M.D. Nave, C.J. Bettles, Deformation microstructures and textures of some cold rolled Mg alloys, Mater. Sci. Eng. A 386 (2008) 205–211.
[5] M.A. Gibson, X. Fang, C.J. Bettles, C.R. Hutchinson, The effect of precipitate state on the creep resistance of Mg-Sn alloys, Scripta Mater. 63 (2010) 899–902.
[6] Y. Lü, Q. Wang, X. Zeng, W. Ding, C. Zhai, Y. Zhu, Effects of rare earths on the microstructure, properties and fracture behavior of Mg-Al alloys, Mater. Sci. Eng. A 278 (2000) 66–76.
[7] T. Al-Samman, X. Li, Sheet texture modification in magnesium-based alloys by selective rare earth alloying, Mater. Sci. Eng. A 528 (2011) 3809–3822.
[8] I.A. Anyanwu, S. Kamado, Y. Kojima, Creep properties of Mg-Gd-Y-Zr alloys, Mater. Trans. 42 (2001) 1212–1218.
[9] A.R. Natarajan, E.L.S. Solomon, B. Puchala, E.A. Marquis, A.V. Ven, On the early stages of precipitation in dilute Mg-Nd alloys, Acta Mater. 108 (2016) 367–379.
[10] D. Zhang, Z. Tan, Q. Huo, Z. Xiao, Z. Fang, X. Yang, Dynamic recrystallization behaviors of Mg-Gd-Y-Zn-Zr alloy with different morphologies and distributions of LPSO phases, Mater. Sci. Eng. A 715 (2018) 389–403.

[11] Z. Yu, C. Xu, J. Meng, S. Kamado, Microstructure evolution and mechanical properties of a high strength Mg-11.7Gd-4.9Y-0.3Zr (wt%) alloy prepared by pre-deformation annealing, hot extrusion and aging, Mater. Sci. Eng. A 703 (2017) 348–358.
[12] C. Xu, J.P. Pan, T. Nakata, X.G. Qiao, Y.Q. Chi, M.Y. Zheng, S. Kamado, Hot compression deformation behavior of Mg-9Gd-2.9Y-1.9Zn-0.4Zr-0.2Ca (wt%) alloy, Mater. Char. 124 (2017) 40–49.
[13] Z. Xiao, Q. Huo, Z. Zhang, W. Huang, L. Luo, Y. Zhang, A. Hashimoto, X. Yang, Influence of pre-straining on creep behaviors of Mg-2Y alloy sheets, J. Alloys Compd. 806 (2019) 19–32.
[14] Y. Zhang, Z. Xiao, Q. Huo, L. Luo, K. Li, A. Hashimoto, X. Yang, Effects of initial texture on the three-dimensional creep anisotropic behaviors of dilute Mg-Y binary alloy sheets, Mater. Sci. Eng. A 766 (2019) 138336.
[15] Y. Shi, L. Luo, Q. Huo, J. Wang, Z. Xiao, J. Guo, X. Yang, Enhancing creep properties of a hot-rolled Mg-4Y binary alloy via a new thought of inhibiting cross-slip, Mater. Char. 147 (2019) 64–71.
[16] X. Wan, Y. Sun, F. Xue, J. Bai, W. Tao, Effects of Sr and Ca on the microstructures and properties of Mg-12Zn-4Al-0.3Mn alloy, Mater. Sci. Eng. A 508 (2009) 50–58.
[17] E. Mohammadi Mazraeshahi, B. Nami, S.M. Miresmaeili, S.M. Tabatabaei, Effect of Si on the creep properties of AZ61 cast magnesium alloy, Mater. Des. 76 (2015) 64–70.
[18] L. Yuan, W. Shi, W. Jiang, Z. Zhao, D. Shan, Effect of heat treatment on elevated temperature tensile and creep properties of the extruded Mg-6Gd-4Y-Nd-0.7Zr alloy, Mater. Sci. Eng. A 658 (2016) 339–347.
[19] H. Sato, K. Sawada, K. Maruyama, H. Oikawa, Improvement of creep rupture life by high temperature pre-creep in magnesium-aluminum binary solid solutions, Mater. Sci. Eng. A 319–321 (2001) 746–750.
[20] T. Honma, T. Ohkubo, S. Kamado, K. Hono, Effect of Zn additions on the age-hardening of Mg-2.0Gd-1.2Y-0.2Zr alloys, Acta Mater. 55 (2007) 4137–4150.
[21] T. Honma, N. Kunito, S. Kamado, Fabrication of extraordinary high-strength magnesium alloy by hot extrusion, Scripta Mater. 61 (2009) 644–647.
[22] J. Gröbner, M. Hampl, R. Schmid-Fetzer, M.A. Easton, S.M. Zhu, M.A. Gibson, J. F. Nie, Phase analysis of Mg-La-Nd and Mg-La-Ce alloys, Intermetallics 28 (2012) 92–101.
[23] C.N. Chiu, J. Gröbner, A. Kozlov, R. Schmid-Fetzer, Experimental study and thermodynamic assessment of ternary Mg-Zn-Ce phase relations focused on Mg-rich alloys, Intermetallics 18 (2010) 399–405.
[24] Y. Yang, X. Yang, Z. Xiao, D. Zhang, J. Wang, T. Sakai, Annealing behavior of a cast Mg-Gd-Y-Zr alloy with necklace fine grains developed under hot deformation, Mater. Sci. Eng. A 688 (2017) 280–288.
[25] Z. Xiao, X. Yang, Y. Yang, Z. Zhang, D. Zhang, Y. Li, T. Sakai, Microstructural development under interrupted hot deformation and the mechanical properties of a cast Mg-Gd-Y-Zr alloy, Mater. Sci. Eng. A 652 (2016) 377–383.
[26] I.H. Jung, M. Sanjari, J. Kim, S. Yue, Role of RE in the deformation and recrystallization of Mg alloy and a new alloy design concept for Mg-RE alloys, Scripta Mater. 102 (2015) 1–6.
[27] T. Sakai, A. Belyakov, R. Kaibyshev, H. Miura, J.J. Jonas, Dynamic and post-dynamic recrystallization under hot, cold and severe plastic deformation conditions, Prog. Mater. Sci. 60 (2014) 130–207.
[28] Q. Huo, X. Yang, H. Sun, B. Li, J. Qin, J. Wang, J. Ma, Enhancement of tensile ductility and stretch formability of AZ31 magnesium alloy sheet processed by cross-wavy bending, J. Alloys Compd. 581 (2013) 230–235.
[29] Q. Huo, X. Yang, J. Ma, H. Sun, J. Qin, Y. Jiang, Microstructural and textural evolution of AZ61 magnesium alloy sheet during bidirectional cyclic bending, Mater. Char. 79 (2013) 43–51.
[30] J.G. Wang, L.M. Hsiung, T.G. Nieh, M. Mabuchi, Creep of a heat treated Mg-4Y-3RE alloy, Mater. Sci. Eng. A 315 (2001) 81–88.
[31] H.K. Kim, W.J. Kim, Creep behavior of AZ31 magnesium alloy in low temperature range between 423 K and 473 K, J. Mater. Sci. 42 (2007) 6171–6176.
[32] S.M. Zhu, M.A. Easton, M.A. Gibson, M.S. Dargusch, J.F. Nie, Analysis of the creep behaviour of die-cast Mg-3Al-1Si alloy, Mater. Sci. Eng. A 578 (2013) 377–382.
[33] M. Celikin, A.A. Kaya, R. Gauvin, M. Pekguleryuz, Effects of manganese on the microstructure and dynamic precipitation in creep-resistant cast Mg-Ce-Mn alloys, Scripta Mater. 66 (2012) 737–740.
[34] Z. Fang, Q. Huo, J. Wang, Z. Xiao, D. Zhang, W. Huang, M. Zhao, X. Yang, Creep behaviors of hot compressed Mg-4Y-2Nd-0.2Zn-0.5Zr alloy with and without aging, Mater. Sci. Eng. A 708 (2017) 460–468.
[35] B. Chen, P.E.J. Flewitt, D.J. Smith, C.P. Jones, An improved method to identify grain boundary creep cavitation in 316H austenitic stainless steel, Ultramicroscopy 111 (2011) 309–313.
[36] Z. Hu, Z. Zhang, Investigation the effect of precipitating characteristics on the creep behavior of HR3C austenitic steel at 650°C, Mater. Sci. Eng. A 742 (2019) 451–463.
[37] Z. Wang, Y. Li, H. Zhao, L. Chen, Z. Zhang, D. Shen, M. Wang, Evolution of μ phase in a Ni-based alloy during long-term creep, J. Alloys Compd. 782 (2019) 1–5.
[38] J.W. Lee, D.J. Kim, H.U. Hong, A new approach to strengthen grain boundaries for creep improvement of a Ni-Cr-Co-Mo superalloy at 950°C, Mater. Sci. Eng. A 625 (2015) 164–168.
[39] L. Yuan, W. Shi, Y. Zhong, D. Shan, Effect of precipitates on creep behavior of the extruded Mg-9Gd-8Y-2Nd-1.2Zr-T5 at 250°C, Mater. Sci. Eng. A 639 (2015) 274–279.
[40] X. Gao, S.M. Zhu, B.C. Muddle, J.F. Nie, Precipitation-hardened Mg-Ca-Zn alloys with superior creep resistance, Scripta Mater. 53 (2005) 1321–1326.
[41] D. Huang, Y. Chen, Y. Tang, H. Liu, G. Niu, Indentation creep behavior of AE42 and Ca-containing AE41 alloys, Mater. Lett. 61 (2007) 1015–1019.
[42] A. Zindal, J. Jain, S.S. Singh, R. Sarvesha, P. Cizek, M.R. Barnett, Effect of heat treatment variables on the formation of precipitate free zones (PFZs) in Mg-8Al-0.5Zn alloy, Mater. Char. 136 (2018) 175–182.
[43] A. Zindal, J. Jain, R. Prasad, S.S. Singh, Effect of pre-strain and grain size on the evolution of precipitate free zones (PFZs) in a Mg-8Al-0.5Zn alloy, Mater. Lett. 201 (2017) 207–210.
[44] D. Yin, Q. Wang, C.J. Boehlert, V. Janik, Creep and fracture behavior of peak-aged Mg-11Y-5Gd-2Zn-0.5Zr (wt pct), Metall. Mater. Trans. 43 (2012) 3338–3350.
[45] W.F. Xu, Y. Zhang, L.M. Peng, W.J. Ding, J.F. Nie, Formation of denuded zones in crept Mg-2.5Gd-0.1Zr alloy, Acta Mater. 84 (2015) 317–329.
[46] J. Wadsworth, O.A. Ruano, O.D. Sherby, Denuded zones, diffusional creep, and grain boundary sliding, Metall. Mater. Trans. 33A (2002) 219–229.
[47] E.J. Lavernia, T.S. Srivatsan, F.A. Mohamed, Strength, deformation, fracture behavior and ductility of aluminum-lithium alloys, J. Mater. Sci. 25 (1990) 1137–1158.
[48] B.W. Pickles, The creep behavior of heat-treated Magnox ZR-55–Magnesium-0.55 percent Zirconium–in the temperature range 350-450 degrees C, J. Inst. Met. 95 (1967) 333–337.
[49] W. Vickers, P. Greenfield, Diffusion-creep in magnesium alloys, J. Nucl. Mater. 24 (1967) 249–260.
[50] K. Li, Q. Huo, Y. Zhang, C. Zhang, W. Huang, Y. Ye, A. Hashimoto, X. Yang, Effects of aging on the creep properties of hot-compressed Mg-2.5wt%Nd binary alloy, Mater. Sci. Eng. A 771 (2020) 138618.
[51] W. Fu, R.H. Wang, J.Y. Zhang, K. Wu, G. Liu, J. Sun, The effect of precipitates on voiding, twinning, and fracture behaviors in Mg alloys, Mater. Sci. Eng. A 720 (2018) 98–109.
[52] W. Huang, Q. Huo, Z. Fang, Z. Xiao, Y. Yin, Z. Tan, X. Yang, Damage analysis of hot-rolled AZ31 Mg alloy sheet during uniaxial tensile testing under different loading directions, Mater. Sci. Eng. A 710 (2018) 289–299.
[53] L. Luo, Z. Xiao, Q. Huo, Y. Yang, W. Huang, J. Guo, Y. Ye, X. Yang, Enhanced mechanical properties of a hot-extruded AZ80 Mg alloy rod by pre-treatments and post-hot compression, J. Alloys Compd. 740 (2018) 180–193.
[54] J. Wang, L. Luo, Q. Huo, Y. Shi, Z. Xiao, Y. Ye, X. Yang, Creep behaviors of a highly concentrated Mg-18wt%Gd binary alloy with and without artificial aging, J. Alloys Compd. 774 (2019) 1036–1045.
[55] Y.H. Kang, H. Yan, R.S. Chen, Creep behavior and microstructure evolution of sand-cast Mg-4Y-2.3Nd-1Gd-0.6Zr alloy crept at 523–573 K, J. Mater. Sci. Technol. 33 (2017) 79–89.
[56] M. Suzuki, H. Sato, K. Maruyama, H. Oikawa, Creep behavior and deformation microstructures of Mg-Y alloys at 550 K, Mater. Sci. Eng. A 252 (1998) 248–255.